Weakly nonlinear shape oscillations of a viscous drop

Dino Zrnić, Gregor Plohl, Günter Brenn*
Graz University of Technology, Institute of Fluid Mechanics and Heat Transfer, A-8010 Graz, Austria
*Corresponding author: guenter.brenn@tugraz.at

Abstract
We investigate nonlinear oscillations of viscous Newtonian liquid drops for their relevance for transport processes across the liquid-gas interface. Theoretically we adopt the weakly nonlinear approach to account for the influence of the nonlinear motion on the drop oscillation. The theory is in progress. Experiments show a different behaviour for large and for small oscillation amplitudes, seen weakly in the oscillation frequency, but strongly in the damping rate. Liquid material parameters deduced from the oscillations agree well with the expected values when amplitudes are small.

Keywords
Drop shape oscillations, weakly nonlinear analysis, drop oscillation experiments, acoustic drop levitation.

Introduction

Shape oscillations of drops have been of interest in science for basic interest and for their relevance for transport processes since more than 140 years. In the appendix to paper [1], Rayleigh presented an analysis of linear shape oscillations of an inviscid drop in a vacuum around a spherical equilibrium state. One result is the equation for the angular frequency of oscillation of the drop deformed according to mode m assuming natural values $m = 2,\ 3,\ 4,\ \ldots$. In [2, 3], Lamb generalised Rayleigh's result by accounting for the drop viscosity and the density of the ambient medium. The threshold Ohnesorge number $Oh = \mu/(\sigma a \rho)^{1/2}$ of the drop for the onset of aperiodic behaviour is predicted. A further generalisation of the analysis of linear drop shape oscillations was achieved in [4] by account for both the viscous and the inertial influences from the ambient medium hosting the viscous oscillating drop. The important aspect of the initiation of the drop oscillations in a drop initially at rest was analysed in [5, 6, 7] where Prosperetti treated the motion as an initial-value problem. He showed that the analyses of linear drop oscillations by the normal-mode approach used in all investigations before may miss the fact that, in a range of Ohnesorge numbers, oscillations starting aperiodically may turn into periodic with ongoing time. The most important results of the here cited highlight papers are the angular frequency and damping rate of the oscillation, as well as the shapes of the deformed drops in linear motion.
First computational investigations of nonlinear drop shape oscillations with large amplitudes are due to [8]. Thereafter, [9] investigated nonlinear oscillations of inviscid drops and bubbles. They found shapes deviating from the linear results, and angular frequencies decreasing with increasing oscillation amplitude (for a maximum prolate aspect ratio of 1.4 by approx. 5%). The sinusoidal dependency of the shape on time is lost with increasing oscillation amplitude. Similar results were reported by [8] already.
The aim of the work in progress reported here is to extend the above investigations to a nonlinear description of shape oscillations of viscous, Newtonian drops. We report the theoretical approach which is analogous to the recently published weakly nonlinear stability analysis of a Newtonian liquid jet ([10]). Experimentally we look at the influence of the initial amplitude on the shape oscillations of acoustically levitated drops. Liquid material parameters deduced are compared to the expected values from the literature.

Theory - formulation of the problem

We study the weakly nonlinear shape oscillations of a viscous liquid drop as sketched in Figure 1. The drop is assumed to be axisymmetric with respect to the azimuthal coordinate φ of the spherical coordinate system. The liquid is treated as incompressible and Newtonian. The dynamic influence from the ambient air is neglected, i.e. we treat the ambience as a vacuum, as will be discussed later in the paper. Body forces are not accounted for, since the Froude number is large. The problem is formulated in spherical coordinates to account for its geometry.
The variables and equations of change are non-dimensionalized with the undeformed drop radius a, the capillary time scale $(\rho a^3/\sigma)^{1/2}$ and the capillary pressure σ/a for length, time and pressure, respectively. Here, ρ is the liquid density and σ the air-liquid interfacial tension. The drop surface is described as a place where $r_s(t,\theta) = 1 + \eta(t,\theta)$, with the non-dimensional deformation η against the undisturbed spherical shape (cf. Figure 1).
For the problem at hand, the equation of continuity and the two components of the momentum equation in the radial (r) and polar angular (θ) directions read

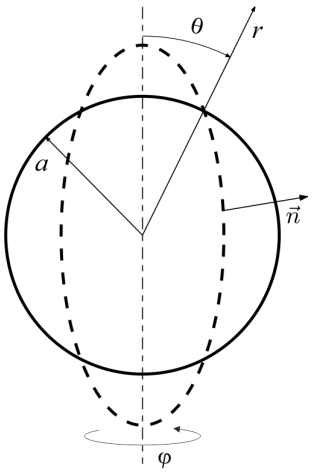

Figure 1. Sketch of the geometry of a liquid drop under deformation at mode 2.

$$\frac{1}{r^2}\frac{\partial}{\partial r}\left(r^2 u_r\right)+\frac{1}{r\sin\theta}\frac{\partial}{\partial\theta}\left(u_\theta\sin\theta\right) = 0 \tag{1}$$

$$\frac{\partial u_r}{\partial t}+u_r\frac{\partial u_r}{\partial r}+\frac{u_\theta}{r}\frac{\partial u_r}{\partial\theta}-\frac{u_\theta^2}{r} = -\frac{\partial p}{\partial r}+Oh\left[\frac{1}{r^2}\frac{\partial^2}{\partial r^2}\left(r^2 u_r\right)+\frac{1}{r^2\sin\theta}\frac{\partial}{\partial\theta}\left(\frac{\partial u_r}{\partial\theta}\sin\theta\right)\right] \tag{2}$$

$$\begin{aligned}\frac{\partial u_\theta}{\partial t}+u_r\frac{\partial u_\theta}{\partial r}+\frac{u_\theta}{r}\frac{\partial u_\theta}{\partial\theta}+\frac{u_r u_\theta}{r} &= -\frac{1}{r}\frac{\partial p}{\partial\theta}+ \\ &+ Oh\left[\frac{1}{r^2}\frac{\partial}{\partial r}\left(r^2\frac{\partial u_\theta}{\partial r}\right)+\frac{1}{r^2}\frac{\partial}{\partial\theta}\left(\frac{1}{\sin\theta}\frac{\partial}{\partial\theta}\left(u_\theta\sin\theta\right)\right)+\frac{2}{r^2}\frac{\partial u_r}{\partial\theta}\right]\end{aligned} \tag{3}$$

where $Oh=\mu/(\sigma a\rho)^{1/2}$ is the Ohnesorge number, the characteristic dimensionless parameter distinguishing the viscous from the inviscid case, with the liquid dynamic viscosity μ. The above set of equations must be solved subject to initial and boundary conditions. The kinematic boundary condition states that the material rate of deformation of the drop surface equals the radial velocity component at the place of the deformed surface, i.e.,

$$u_r=\frac{D\eta}{Dt}=\frac{\partial\eta}{\partial t}+\frac{u_\theta}{r}\frac{\partial\eta}{\partial\theta}\quad\text{at}\ \ r=1+\eta \tag{4}$$

The first dynamic boundary condition states that the shear stress at the drop surface is zero, since the ambient gas phase dynamic viscosity is very small, so that momentum cannot be transferred across the drop boundary at an appreciable rate. The second dynamic boundary condition states that the stress normal to the drop surface, composed from the flow-induced pressure and a viscous contribution, differs across the interface by the contribution due to the surface tension. The zero-shear stress boundary condition reads

$$(\vec{n}\cdot\tau)\times\vec{n}=\vec{0}\quad\text{at}\ \ r=1+\eta \tag{5}$$

where the outward unit normal vector $\vec{n}$ is given as

$$\vec{n}=\frac{1}{|\vec{\nabla}F|}\vec{\nabla}F\quad\text{with}\ \ F=r-1-\eta(t,\theta)=0 \tag{6}$$

and the viscous extra stress tensor in (5) is the one for the incompressible Newtonian fluid. The corresponding normal stress boundary condition reads

$$-p+Oh\,(\vec{n}\cdot\tau)\cdot\vec{n}+\left(\vec{\nabla}\cdot\vec{n}\right)=0\quad\text{at}\ \ r=1+\eta \tag{7}$$

We obtain the divergence of the normal unit vector in this equation as

$$\left(\vec{\nabla}\cdot\vec{n}\right)=\frac{1}{r}\frac{2+3\left(\frac{1}{r}\frac{\partial\eta}{\partial\theta}\right)^2}{\left[1+\left(\frac{1}{r}\frac{\partial\eta}{\partial\theta}\right)^2\right]^{3/2}}-\frac{1}{r^2\sin\theta}\frac{\partial}{\partial\theta}\left(\frac{\frac{\partial\eta}{\partial\theta}}{\left[1+\left(\frac{1}{r}\frac{\partial\eta}{\partial\theta}\right)^2\right]^{1/2}}\sin\theta\right)\quad\text{at}\ \ r=1+\eta \tag{8}$$

The initial imposed surface disturbance is governed by a Legendre polynomial of degree m with the amplitude η_0. With this assumption, volume conservation leads to the following expression for the initial non-dimensional drop shape:

$$\begin{aligned}r_s(0,\theta) &= 1+\eta(0,\theta)= \\ &= \left(\frac{1}{1+3\eta_0^2/(2m+1)}\right)^{1/3}+\eta_0 P_m(\cos\theta)=1+\eta_0 P_m(\cos\theta)-\frac{1}{2m+1}\eta_0^2+\frac{3}{(2m+1)^2}\eta_0^4\mp\dots\end{aligned} \tag{9}$$

As usual in weakly nonlinear analysis, the initial deformation amplitude is assumed to be small, i.e. $\eta_0 \ll 1$. For analyzing these equations in a weakly nonlinear form, the two velocity components and the pressure in the flow field, as well as the deformed interface shape, are expanded in power series with respect to the small deformation parameter η_0. We therefore formulate the expansions of the flow field properties, e.g., u_r and p as

$$u_r = u_{r1}\eta_0 + u_{r2}\eta_0^2 + \dots \tag{10}$$

$$p = p_1\eta_0 + p_2\eta_0^2 + \dots \tag{11}$$

Furthermore, one important difference between the linear analysis and the present weakly nonlinear one is that the boundary conditions are satisfied on the deformed drop surface, not on the undeformed spherical shape. For doing this, but still allowing for the functions in the boundary conditions to be evaluated on the undeformed drop surface, their values on the deformed shape are represented by Taylor expansions, such as, e.g., for u_r and p,

$$u_r|_{r=1+\eta} = u_r|_{r=1} + \left.\frac{\partial u_r}{\partial r}\right|_{r=1}\eta + \dots \tag{12}$$

$$p|_{r=1+\eta} = p|_{r=1} + \left.\frac{\partial p}{\partial r}\right|_{r=1}\eta + \dots \tag{13}$$

Substituting these approaches into the equations of change (1) - (3) and into the boundary conditions (4), (5) and (7), and representing the flow properties and their derivatives as given in (10) through (13), we obtain sets of first and second order equations of motion, with the boundary conditions, consisting of all the terms with the deformation parameter η_0 to the first and second powers, respectively.

First-order equations

To obtain the first-order equations we collect all the terms in the above expansions with the parameter η_0 to the first power. The first-order continuity and momentum equations read

$$\frac{1}{r^2}\frac{\partial}{\partial r}\left(r^2 u_{r1}\right) + \frac{1}{r\sin\theta}\frac{\partial}{\partial\theta}\left(u_{\theta 1}\sin\theta\right) = 0 \tag{14}$$

$$\frac{\partial u_{r1}}{\partial t} = -\frac{\partial p_1}{\partial r} + Oh\left[\frac{1}{r^2}\frac{\partial^2}{\partial r^2}\left(r^2 u_{r1}\right) + \frac{1}{r^2\sin\theta}\frac{\partial}{\partial\theta}\left(\frac{\partial u_{r1}}{\partial\theta}\sin\theta\right)\right] \tag{15}$$

$$\frac{\partial u_{\theta 1}}{\partial t} = -\frac{1}{r}\frac{\partial p_1}{\partial\theta} + \tag{16}$$

$$+ \quad Oh\left[\frac{1}{r^2}\frac{\partial}{\partial r}\left(r^2\frac{\partial u_{\theta 1}}{\partial r}\right) + \frac{1}{r^2}\frac{\partial}{\partial\theta}\left(\frac{1}{\sin\theta}\frac{\partial}{\partial\theta}\left(u_{\theta 1}\sin\theta\right)\right) + \frac{2}{r^2}\frac{\partial u_{r1}}{\partial\theta}\right]$$

For the boundary conditions of first order to be satisfied at $r = 1$ we obtain

$$u_{r1} = \frac{\partial\eta_1}{\partial t} \quad \text{kinematic} \tag{17}$$

$$r\frac{\partial}{\partial r}\left(\frac{u_{\theta 1}}{r}\right) + \frac{1}{r}\frac{\partial u_{r1}}{\partial\theta} = 0 \quad \text{zero shear stress} \tag{18}$$

$$-p_1 + 2Oh\frac{\partial u_{r1}}{\partial r} + 2 - \left(2\eta_1 + \frac{\partial\eta_1}{\partial\theta}\cot\theta + \frac{\partial^2\eta_1}{\partial\theta^2}\right) = 0 \quad \text{zero normal stress} \tag{19}$$

Furthermore, the initial conditions of first order are

$$\eta_1(0,\theta) = P_m(\cos\theta) \quad \text{and} \quad \frac{\partial\eta_1}{\partial t}(0,\theta) = 0 \tag{20}$$

Second-order equations

To obtain the second-order equations we collect all the terms in the above expansions with the parameter η_0 to the second power. The second-order continuity and momentum equations read

$$\frac{1}{r^2}\frac{\partial}{\partial r}\left(r^2 u_{r2}\right) + \frac{1}{r\sin\theta}\frac{\partial}{\partial\theta}\left(u_{\theta 2}\sin\theta\right) = 0 \tag{21}$$

$$\frac{\partial u_{r2}}{\partial t} + u_{r1}\frac{\partial u_{r1}}{\partial r} + \frac{u_{\theta 1}}{r}\frac{\partial u_{r1}}{\partial\theta} - \frac{u_{\theta 1}^2}{r} = -\frac{\partial p_2}{\partial r} + Oh\left[\frac{1}{r^2}\frac{\partial^2}{\partial r^2}\left(r^2 u_{r2}\right) + \frac{1}{r^2\sin\theta}\frac{\partial}{\partial\theta}\left(\frac{\partial u_{\theta 2}}{\partial\theta}\sin\theta\right)\right] \tag{22}$$

$$\frac{\partial u_{\theta 2}}{\partial t} + u_{r1}\frac{\partial u_{\theta 1}}{\partial r} + \frac{u_{\theta 1}}{r}\frac{\partial u_{\theta 1}}{\partial\theta} + \frac{u_{r1}u_{\theta 1}}{r} = -\frac{1}{r}\frac{\partial p_2}{\partial\theta} + \tag{23}$$

$$+ \quad Oh\left[\frac{1}{r^2}\frac{\partial}{\partial r}\left(r^2\frac{\partial u_{\theta 2}}{\partial r}\right) + \frac{1}{r^2}\frac{\partial}{\partial\theta}\left(\frac{1}{\sin\theta}\frac{\partial}{\partial\theta}\left(u_{\theta 2}\sin\theta\right)\right) + \frac{2}{r^2}\frac{\partial u_{r2}}{\partial\theta}\right]$$

The boundary conditions of second order at $r = 1$ are

$$u_{r2} - \frac{\partial \eta_2}{\partial t} = \frac{u_{\theta 1}}{r}\frac{\partial \eta_1}{\partial \theta} - \eta_1 \frac{\partial u_{r1}}{\partial r} \quad \text{kinematic} \tag{24}$$

$$r\frac{\partial}{\partial r}\left(\frac{u_{\theta 2}}{r}\right) + \frac{1}{r}\frac{\partial u_{r2}}{\partial \theta} = -\eta_1 \frac{\partial}{\partial r}\left(r\frac{\partial}{\partial r}\left(\frac{u_{\theta 1}}{r}\right) + \frac{1}{r}\frac{\partial u_{r1}}{\partial \theta}\right) - 2\left(r\frac{\partial}{\partial r}\left(\frac{u_{r1}}{r}\right) - \frac{1}{r}\frac{\partial u_{\theta 1}}{\partial \theta}\right)\frac{1}{r}\frac{\partial \eta_1}{\partial \theta} \quad \text{zero shear stress} \tag{25}$$

$$-p_2 + 2Oh\frac{\partial u_{r2}}{\partial r} - \left(2\eta_2 + \frac{\partial \eta_2}{\partial \theta}\cot\theta + \frac{\partial^2 \eta_2}{\partial \theta^2}\right) = \eta_1 \frac{\partial p_1}{\partial r} - \tag{26}$$

$$-2Oh\left[\eta_1\frac{\partial^2 u_{r1}}{\partial r^2} - \frac{1}{r}\frac{\partial \eta_1}{\partial \theta}\left(r\frac{\partial}{\partial r}\left(\frac{u_{\theta 1}}{r}\right) + \frac{1}{r}\frac{\partial u_{r1}}{\partial \theta}\right)\right] - \left(2\eta_1^2 + 2\eta_1\frac{\partial \eta_1}{\partial \theta}\cot\theta + 2\eta_1\frac{\partial^2 \eta_1}{\partial \theta^2}\right) \quad \text{zero normal stress}$$

Furthermore, the initial conditions of second order are

$$\eta_2(0,\theta) = -\frac{1}{2m+1} \quad \text{and} \quad \frac{\partial \eta_2}{\partial t}(0,\theta) = 0 \tag{27}$$

Solving these sets of equations will reveal the weakly nonlinear role of the viscous stresses in the drop liquid on the shape oscillations of a Newtonian viscous liquid drop in a vacuum.

Solutions

First-order solutions

We describe the two-dimensional flow field in the drop by the Stokesian stream function ψ. Introducing it into the first-order linearised momentum equation by the definitions

$$u_{r1} = -\frac{1}{r^2 \sin\theta}\frac{\partial \psi}{\partial \theta} \quad \text{and} \quad u_{\theta 1} = \frac{1}{r\sin\theta}\frac{\partial \psi}{\partial r} \tag{28}$$

and taking the curl of the resulting equation, we obtain the fourth-order partial differential equation

$$\left(\frac{1}{Oh}\frac{\partial}{\partial t} - E_s^2\right)\left(E_s^2 \psi\right) = 0 \tag{29}$$

with the operator [11]

$$E_s^2 = \frac{\partial^2}{\partial r^2} + \frac{\sin\theta}{r^2}\frac{\partial}{\partial \theta}\left(\frac{1}{\sin\theta}\frac{\partial}{\partial \theta}\right) . \tag{30}$$

The resulting stream function ψ consists of two contributions $\psi_1 + \psi_2$ [12] represented by the proportionalities

$$\psi_1 \propto r^{m+1}\sin^2\theta P_m'(\cos\theta)e^{-\alpha_m t} \quad \text{and} \quad \psi_2 \propto qrj_m(qr)\sin^2\theta P_m'(\cos\theta)e^{-\alpha_m t} \tag{31}$$

where $P_m'(\cos\theta)$ is the first-order derivative of the Legendre polynomial P_m with respect to its argument and j_m is a spherical Bessel function of the first kind and order m. In its argument we have defined $q = \sqrt{\alpha_m/Oh}$. The radial and angular components of the velocity vector follow as derivatives of the stream function.

$$u_{r1} = -\left[C_{1m}r^{m-1} + C_{2m}q\frac{j_m(qr)}{qr}\right]m(m+1)P_m(\cos\theta)e^{-\alpha_m t} \tag{32}$$

and

$$u_{\theta 1} = \left[C_{1m}(m+1)r^{m-1} + C_{2m}q\left((m+1)\frac{j_m(qr)}{qr} - j_{m+1}(qr)\right)\right]\sin\theta P_m'(\cos\theta)e^{-\alpha_m t} , \tag{33}$$

respectively. The two integration constants C_1 and C_2 are determined by the first-order kinematic and zero shear stress boundary conditions and read

$$C_{1m} = \frac{\hat{\eta}_1\alpha_m}{m(m+1)}\left[1 + \frac{2\left(m^2-1\right)}{2qj_{m+1}(q)/j_m(q) - q^2}\right] \qquad C_{2m} = -\frac{2(m-1)\hat{\eta}_1\alpha_m}{m[2qj_{m+1}(q) - q^2 j_m(q)]} \tag{34}$$

The pressure field is obtained by integration of one component of the momentum equation as

$$p = -C_{1m}(m+1)\alpha_m r^m P_m e^{-\alpha_m t} . \tag{35}$$

The characteristic equation for the complex angular frequency α_m is now found from the zero normal stress boundary condition of first order (26) and reads

$$\frac{\alpha_{m,0}^2}{\alpha_m^2} = \frac{2(m^2-1)}{q^2 - 2qj_{m+1}/j_m} - 1 + \frac{2m(m-1)}{q^2}\left[1 + \frac{2(m+1)j_{m+1}/j_m}{2j_{m+1}/j_m - q}\right] \tag{36}$$

where we have denoted $\alpha_{m,0} = [m(m-1)(m+2)]^{1/2}$. The spherical Bessel functions are taken at the value q of their arguments. The equation is identical to the results of [2] and [13].

Second-order solutions

The general solution for, e.g., the second-order pressure is sought as a sum of two contributions

$$p_2(r,\theta,t) = p_{21}(r,\theta,t) + p_{22}(r,\theta,t) \tag{37}$$

where subscript 21 indicates the solution of the second-order equations system including non-linear first-order term products, and subscript 22 the solutions of the homogeneous system.

The contributions to the second-order solutions with subscripts 21 are first determined. Considering the second-order equations of motion (21)-(23) we see that it is convenient to eliminate the second-order velocities from the momentum equations using the continuity equation (21) to obtain a differential equation for the second-order pressure p_{21}. The resulting equation reads

$$\frac{1}{r^2}\frac{\partial}{\partial r}\left(r^2\frac{\partial p_{21}}{\partial r}\right) + \frac{1}{r\sin\theta}\frac{\partial}{\partial\theta}\left(\frac{\sin\theta}{r}\frac{\partial p_{21}}{\partial\theta}\right) = -\frac{1}{r^2}\frac{\partial}{\partial r}\left[r^2\left(u_{r1}\frac{\partial u_{r1}}{\partial r} + \frac{u_{\theta 1}}{r}\frac{\partial u_{r1}}{\partial\theta} - \frac{u_{\theta 1}^2}{r}\right)\right] \tag{38}$$

$$- \frac{1}{r\sin\theta}\frac{\partial}{\partial\theta}\left[\left(u_{r1}\frac{\partial u_{\theta 1}}{\partial r} + \frac{u_{\theta 1}}{r}\frac{\partial u_{\theta 1}}{\partial\theta} + \frac{u_{r1}u_{\theta 1}}{r}\right)\sin\theta\right] \tag{39}$$

which we re-formulate into the compact form

$$\Delta p_{21} = -\mathrm{div}\left[\left(\vec{v}_1\cdot\vec{\nabla}\right)\vec{v}_1\right] \tag{40}$$

In this equation, $\vec{v}_1$ represents the first-order velocity field. With the Lamé identity, equation (40) becomes

$$\Delta p_{21} = -\mathrm{div}\left[\vec{\nabla}\vec{v}_1^2/2 - \vec{v}_1\times\left(\vec{\nabla}\times\vec{v}_1\right)\right] \tag{41}$$

which, for our present flow field, may be re-written as

$$\Delta\left[p_{21} + \vec{v}_1^2/2\right] = -\frac{\alpha_m}{Oh}\mathrm{div}\left[\frac{\psi_2}{r^2}\vec{\nabla}\psi\right] \tag{42}$$

This is a Poisson equation for the modified pressure $\mathcal{P}_{21} = p_{21} + \vec{v}_1^2/2$ [10]. The structure of the solution in terms of its dependency on the polar angular coordinate and on time is determined by $\vec{v}_1^2$ and the products of first-order terms on the right-hand side of equation (42). Both groups of terms contain exponential functions of $-2\alpha_m t$. In solving the Poisson equation, the exact general homogeneous solution is first determined, and a particular solution is obtained by approximating with a polynomial function the terms on the right-hand side of the equation for a given value of mode m of the initial deformation, which contains products of spherical Bessel functions of different orders. The approximation is needed, since an exact form of the particular solution seems to be out of reach. Increasing order of the approximation raises the accuracy of the approximation. The complete solutions of second order for all the flow field variables remain to be found.

Experiments, materials and methods

For investigating experimentally the damped oscillations of drops of Newtonian liquids the technique of acoustic levitation was used [15]. The levitation of individual drops was achieved using an ultrasonic levitator. The device suspends the drop in a fixed position contactlessly and allows various physical processes to be investigated without any influences from contacting mechanical parts.

A syringe with a thin needle was used to produce the drops of the test liquids. The diameters of the drops were in the range between 1 mm and 3 mm. A high-speed camera was used to record the images of the levitated drop under back-light illumination at framing rates up to 4 kHz. The resolution of the acquired images was 300 Pxl/mm with the uncertainty of $\pm$2 Pxl.

Oscillations of the levitated object are excited by amplitude-modulating the ultrasound near the resonance frequency of the base mode $m = 2$. The oscillation amplitude during the excitation was around 10% of the equilibrium drop radius. After the modulation is switched off, the drop performs damped oscillations. During the experiments, the carrier signal driving the acoustic transducer was always active. The experiment yields the drop radius and both the angular frequency and the damping rate of the drop shape oscillations. For further details the reader is referred to [15, 16, 17].

The experiments were performed with aqueous glycerol solutions. The solutions were prepared in demineralized water with different glycerol mass fractions. The dynamic viscosity μ^* of the solutions was measured with a capillary viscometer and the surface tension σ^* with a pendant drop tensiometer. The density of the solutions was determined by weighing a known volume of the test liquids. The liquid properties measured at the temperature of 24°C are listed in Table 1 and are in good agreement with values known from the literature [14].

Table 1. Properties of the aqueous glycerol solutions at 24°C.

Glycerol mass fraction w [wt.%]	Density ρ [kg/m^3]	Surface tension σ^* [N/m]	Viscosity μ^* [mPa s]
20	1045 $\pm 1\%$	0.069 $\pm 4\%$	1.62 $\pm 1\%$
30	1068 $\pm 1\%$	0.067 $\pm 4\%$	2.23 $\pm 1\%$
50	1121.5 $\pm 1\%$	0.065 $\pm 4\%$	5.25 $\pm 1\%$
65	1161 $\pm 1\%$	0.063 $\pm 4\%$	11.75 $\pm 1\%$

From the recorded images of drop shape oscillations the height and width of the drop as functions of time are obtained. The oscillation shown in Figure 2 was obtained for a 20 wt.% solution drop with the equilibrium diameter of 2.05 mm. The time-dependent distance $y(t)$ between the north and south poles of the drop, that is the height of the drop, and equivalently the width of the drop, are represented by a function $y(t) = y_0 + A\cos(\alpha_{2,i}t + \varphi_0)\cdot \mathrm{e}^{-\alpha_{2,r}t}$, which is a general description of a damped oscillation [17]. In this function, y_0 is the equilibrium height (or the equilibrium width of the drop), $\alpha_{2,i}$ is the angular oscillation frequency, t is time, A the oscillation amplitude at time $t = t_0$ from which on the data is modeled, φ_0 is a reference phase angle and $\alpha_{2,r}$ is the damping rate of the fundamental mode $m = 2$. The oscillations were fitted in both directions of deformation, as shown in Figure 2(right). As results of the measurements, the average values for the frequency and the damping rate were obtained. In the case of large deviations between the values obtained in the equatorial and polar directions, the measured results were discarded. The first and the later parts of the oscillation were fitted separately, as shown in Figure 2(left). The first part corresponds to large-amplitude (LA) oscillations and, the later to small-amplitude (SA) oscillations. The complex angular frequency $\alpha_2 = \alpha_{2,r} + i\alpha_{2,i} = \alpha_{2,r} + i2\pi \cdot f$ for the large α_2^{LA} and small α_2^{SA} amplitude oscillations is therefore known.

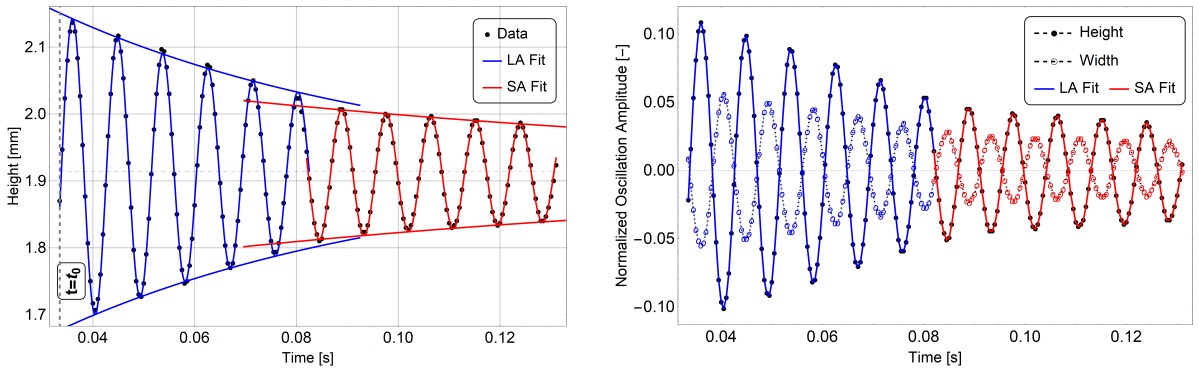

Figure 2. Damped oscillations of a levitated 20 wt.% aqueous glycerol solution drop. (Left) Drop height as a function of time with the fitting curves for the large-amplitude (LA) and for the small-amplitude oscillations (SA). (Right) Normalized oscillation amplitudes as functions of time, with the fitting curves.

Figure 2(right) presents the normalized non-dimensional oscillation amplitudes as functions of time and shows that the oscillation amplitude in the polar direction is always higher than the oscillation amplitude in the equatorial direction. The reason for this difference is due to the difference of the axial and radial forces of the acoustic field. What is termed the amplitude of the oscillations of the drop in the present context is defined as the amplitude in the polar direction.

For the drop oscillation shown in Figure 2, the following values are obtained. The oscillation amplitude in the first part of the motion is about 11.6% of the equilibrium drop radius, and in the last part about 6.9%. The measured complex angular frequencies are $\alpha_2^{LA} = 15\,\mathrm{s}^{-1} + i2\pi \cdot 113\,\mathrm{Hz}$ and $\alpha_2^{SA} = 7\,\mathrm{s}^{-1} + i2\pi \cdot 113.8\,\mathrm{Hz}$. The measured complex frequency α_2 has an uncertainty of $\pm 10\%$ in the damping rate, and of $\pm 1\%$ in the oscillation frequency. This follows from the analysis of the fitting results of the function for the drop height or width to the measured data. The oscillation frequencies for both the SA oscillation and the LA oscillation are nearly the same. However, the damping rate in the case of LA oscillation is nearly double the value of the SA oscillation.

From the measured complex angular frequency, the surface tension σ and the dynamic viscosity μ of the drop liquid are determined [1, 2, 18]. This so-called oscillating drop method for measuring material properties of the drop liquid relies on the linear theory, which is expected to hold if the initial oscillation amplitude is less than 10% of the equilibrium drop radius [18]. The surface tension σ of a drop liquid determines the drop oscillation frequency and the liquid dynamic viscosity μ determines the damping rate. The values are calculated as

$$\sigma = \frac{3\pi\rho V f^2}{m(m-1)(m+2)} \qquad (43) \qquad \mu = \frac{\alpha_{m,r}\rho a^2}{(m-1)(2m+1)}. \qquad (44)$$

Equations (43) and (44) are valid for drops with small Ohnesorge number ($Oh < 0.1$), as pointed out by Prosperetti [7].

Results and discussion

With each of the glycerol solutions, at least 5 oscillation experiments were performed. Measurements were conducted at atmospheric pressure and a room temperature of 24°C. The measured complex angular frequency is first compared to the results provided by the characteristic equation (36) by introducing the non-dimensional complex angular frequency $\Omega = \alpha_2/\alpha_{2,0}$. The comparison presented in Figure 3 shows that the complex angular frequency extracted from the last part of the oscillation, i.e. small-amplitude oscillations, is in good agreement with the results obtained from the characteristic equation. On the other hand, the complex angular frequencies extracted from the large-amplitude oscillations exhibit large deviations from the calculated values. The deviation is more pronounced for the damping rate (Figure 3 right) and less for the oscillation frequency (Figure 3 left). For the non-dimensional oscillation frequency (Figure 3-left) no clear distinction between the SA and LA cases can be made. The reasons for this could be the uncertainties of the liquid properties entering the equation for the dimensional form of $\alpha_{m,0} = [m(m-1)(m+2)\sigma/\rho a^3]$ and the error of the measured oscillation frequency. The difference between the non-dimensional damping rates for the SA and LA cases (Figure 3-right) increases with the Ohnesorge number. The threshold oscillation amplitude of $0.07a$ separating the LA and SA cases is set between the minimum oscillation amplitude extracted from the first part of the motion and the maximum amplitude extracted from the last part of the motion. The results presented in Figure 3 are expected, since the characteristic equation (36) is a result of the linear theory.

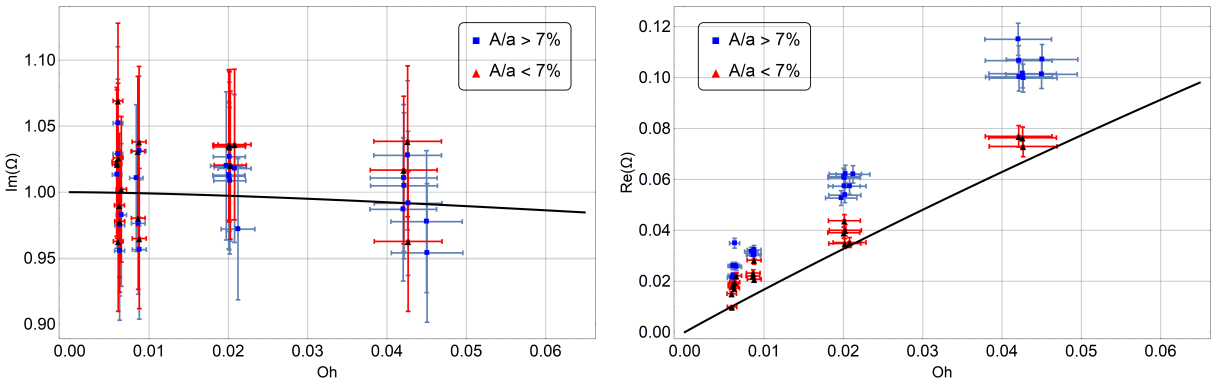

Figure 3. Measured (points) and calculated (solid line) non-dimensional complex angular frequency Ω versus the Ohnesorge number. (Left) Angular frequency, (right) damping rate. Comparison of the results for the large-amplitude (LA) and small-amplitude (SA) oscillations. The threshold oscillation amplitude separating the LA and SA cases is set to $0.07a$.

Next, we analyze the results of the oscillating drop method using equations (43) and (44) for the cases of small and large-amplitude oscillations. Table 2 presents the data for the damped drop oscillation shown in Figure 2. As noted in the previous section, the oscillation frequencies for the SA and LA oscillations are nearly the same. Therefore, the surface tension obtained by equation (43) is nearly the same for both cases and is close to the value σ^* from pendant drop tensiometry. The absolute deviation between the values from the two methods is about 4%, which is of the order of the uncertainties of σ^*. In contrast, the damping rate for the LA oscillation is nearly double the value of SA, which doubles the value of the dynamic viscosity obtained by equation (44) against the LA case. The deviation between the values obtained by the oscillating drop method and capillary viscometry is around 6% in the case of SA oscillations, and around 105% in the case of LA oscillations.

Table 2. Data for the 20 wt.$\%$ glycerol solution drop oscillation shown in Figure 2. The equilibrium drop radius is $1.025\,\mathrm{mm}$, the corresponding inviscid eigenfrequency is $\alpha_{2,0} = 2\pi \cdot 115\mathrm{Hz}$, and the Ohnesorge number is 0.006.

	f [Hz]	$\alpha_{2,r}$ [1/s]	Im(Ω) [−]	Re(Ω) [−]	A/a [%]	σ [N/m]	μ [mPa s]
Small-amplitude oscillations	113.8	7	1.02	0.01	6.9	0.072	1.52
Large-amplitude oscillations	113	15	1.013	0.022	11.6	0.071	3.33

The average values of surface tension and dynamic viscosity of the investigated aqueous glycerol solutions obtained by the oscillating drop method are presented in Table 3. The values of surface tension σ obtained by equation (43) for both small and large-amplitude oscillations are in excellent agreement with the values σ^* from pendant drop tensiometry. The reason is that the oscillation frequencies for SA and LA oscillations are nearly equal. The maximum absolute deviation between the oscillating drop method and the pendant drop tensiometry is within 4.7% which is of the order of the uncertainties of σ^*. The values of the dynamic viscosity μ obtained by equation (44) show strong dependency on the oscillation amplitude. The absolute deviation between the methods decreases with increasing glycerol mass fraction.

Table 3. Surface tension σ and dynamic viscosity μ of aqueous glycerol solution drops from equations (43) and (44). Results of SA and LA oscillations with corresponding absolute deviations between values from the oscillating drop method and from Table 1.

Glycerol mass fraction $w\,[\mathrm{wt.\%}]$	SA oscillations		LA oscillations	
	Surface tension $\sigma\,[\mathrm{N/m}]\left(\frac{\lvert\Delta\sigma\rvert}{\sigma^*}\right)$	Dynamic viscosity $\mu\,[\mathrm{mPa\,s}]\left(\frac{\lvert\Delta\mu\rvert}{\mu^*}\right)$	Surface tension $\sigma\,[\mathrm{N/m}]\left(\frac{\lvert\Delta\sigma\rvert}{\sigma^*}\right)$	Dynamic viscosity $\mu\,[\mathrm{mPa\,s}]\left(\frac{\lvert\Delta\mu\rvert}{\mu^*}\right)$
20	0.069 $(<1\%)$	2.4 (48%)	0.068 (1.5%)	3.75 (132%)
30	0.068 $(<1\%)$	3.3 (48%)	0.066 (1.4%)	4.56 (105%)
50	0.068 (4.6%)	5.58 (6.8%)	0.067 (3.7%)	8.53 (53%)
65	0.064 (1.6%)	11.84 $(<1\%)$	0.062 (1.5%)	15.9 (35%)

Conclusions

The present study lays the framework for the weakly nonlinear theory of Newtonian drop shape oscillations. The oscillating drop method was used to demonstrate the limits of validity of the linear theory of drop shape oscillations. According to Becker *et al.* [18], the linear theory is expected to hold if the initial oscillation amplitude is less than 10% of the equilibrium drop radius. Our experimental results show, however, that, even for an initial oscillation amplitude around 7% of the equilibrium drop radius, large deviations from the linear theory can occur. These deviations are more pronounced in the damping rate, while the oscillation frequency is practically unaffected by the initial amplitude.

Acknowledgements

Financial support of this research project by the Austrian Science Fund - FWF - through project number I3326-N32 in the DACH framework is gratefully acknowledged.

Nomenclature

A	oscillation amplitude [m]	$\vec{v_1}$	first-order velocity field
a	equilibrium drop radius [m]	w	glycerol mass fraction [wt.%]
f	damped oscillation frequency [Hz]	$y(t)$	time-dependent distance [m]
j_m, j_{m+1}	spherical Bessel functions [1]	y_0	equilibrium drop height or width [m]
m	mode number [1]	α_m=$\alpha_{m,r}$+$i\alpha_{m,i}$	complex angular frequency [s^{-1}]
$\vec{n}$	outward unit normal vector	$\alpha_{m,0}$	inviscid angular frequency [s^{-1}]
Oh	Ohnesorge number	$\alpha_{m,r}$	damping rate mode m [s^{-1}]
p	pressure [Pa]	$\dot{\gamma}$	rate of deformation tensor [s^{-1}]
P_m	Legendre polynomial	η	surface deformation
$p_1,\ p_2$	1st-, 2nd-order pressure	$\hat{\eta}_1$	oscillation amplitude [m]
$r,\ \theta,\ \phi$	spherical coordinates	μ	dynamic viscosity [Pa s]
r_s	drop shape	ρ	density [kg m^{-3}]
t	time [s]	σ	surface tension [N m^{-1}]
$u_{r1},\ u_{r2}$	1st-, 2nd-order radial velocity	τ	extra stress tensor [Pa]
$u_{\theta 1},\ u_{\theta 2}$	1st, 2nd-order polar velocity	φ_0	reference phase angle [rad]
V	drop volume [m^3]	ψ	Stokesian stream function

References

[1] Rayleigh, J.W.S., 1879, *Proc. R. Soc. London A*, 29, pp. 71-97.
[2] Lamb, Sir H., 1881, *Proc. London Math. Soc.*, 13, pp. 51-66.
[3] Lamb, Sir H., 1936, Hydrodynamics 6th edn., Cambridge.
[4] Miller, C.A., Scriven, L.E., 1968, *J. Fluid Mech.*, 32, pp. 417-435.
[5] Prosperetti, A., 1977, *Quart. Appl. Math.* 35, pp. 339-352.
[6] Prosperetti, A., 1980, *J. Méc.*, 19, pp. 149-182.
[7] Prosperetti, A., 1980, *J. Fluid Mech.*, 100, pp. 333-347.
[8] Foote, G.B., 1973, *J. Comp. Phys.*, 11, pp. 507-530.
[9] Tsamopoulos, J.A., Brown, R.A., 1983, *J. Fluid Mech.*, 127, pp. 519-537.
[10] Renoult, M.-C., Brenn, G., Plohl, G., Mutabazi, I., 2018, *J. Fluid Mech.*, 856, pp. 169-201.
[11] Bird, R.B., Stewart, W.E., Lightfoot, 1962, Transport Phenomena, Wiley New York.
[12] Tomotika, S., 1935, *Proc. R. Soc. London A*, 150, pp. 322-337.
[13] Chandrasekhar, S., 1959, *Proc. London Math. Soc.*, 9, pp. 141-149.
[14] Takamura, K., Fischer, H., Morrow, N.R., 2012, *J. Petrol. Sci. Eng.*, 98, pp. 50-60.
[15] Yarin, A., Brenn, G., Kastner, O., Rensink, D., Tropea, C. , 1999, *J. Fluid Mech.*, 399, pp. 151-204.
[16] Brenn, G., Teichtmeister, S., 2013, *J. Fluid Mech.*, 733, pp. 504-527.
[17] Brenn, G., Plohl, G., 2015, *J. Non-Newton. Fluid Mech.*, 223, pp. 88-97.
[18] Becker, E., Hiller, W.J., Kowalewski, T.A., 1991, *J. Fluid Mech.*, 231, pp. 189-210.